MHD-Stability of magnetotail equilibria including a background pressure

K. Schindler

Fakultät für Physik und Astronomie, Ruhr-Universität Bochum, Germany

J.Birn

Los Alamos National Laboratory, Los Alamos, New Mexico

Short title: MHD STABILITY OF MAGNETOTAIL

Abstract. This paper deals with ideal-MHD stability of equilibrium configurations modelling the plasma sheet of the Earth's magnetotail. The approach exploits the fact that in the absence of a cross-tail magnetic field component the MHD stability problem for 2D equilibria under general 3D perturbations can be reduced to analyzing stability with respect to ballooning modes alone. The correspondingly specialized MHD energy principle is numerically minimized for three different equilibrium models. In all cases the stability of symmetric modes was governed by the interchange criterion based on entropy. A constant background pressure is included, which, even if small, can have a significant stabilizing effect. An analytical approach provides a set of rather simple stability criteria, which are consistent with the numerical minimization results. A main conclusion is that configurations with realistic tailward pressure profiles are found stable. Also, the entropy criterion implies that stability transitions cannot occur during the adiabatic evolution of ideal-MHD tail configurations.

1. Introduction

The plasma sheet of the Earth's magnetotail is a site of pronounced temporal variations. There are time intervals of relatively quiet states, which suddenly turn into periods with intense fluctuations and large scale temporal evolution. Observations point at the plasma sheet as the location of the onset of processes directly related to magnetospheric activity, particularly magnetospheric substorms, involving large mass and energy transport [*Sergeev et al.*, 1993; *Angelopoulos et al.*, 1996; *Baker et al.*, 1997; *Miyashita et al.*, 2000, 2001]. Several instabilities have been suggested as candidates for onset processes, among them tearing modes [*Schindler*, 1974; *Kuznetsova and Zelenyi*, 1991; *Birn*, 1980; *Baker et al.*, 1996; *Hesse and Schindler*, 2001], several microinstabilities [*Lui et al.*, 1990] and ideal MHD modes [*Miura*, 2001].

A typical scenario assumes an initial state with a wide plasma sheet with widths much larger than the intrinsic ion scales, such as the ion inertial length, which generally lie in the range of 100-1000 km. Such states have been described successfully by ideal MHD [e.g. *Schindler and Birn*, 1978]. During the growth phase of the magnetospheric substorm cycle the plasma sheet develops thin current sheets [*Kaufmann*, 1987; *Mitchell et al.*, 1990; *Sergeev et al.*, 1990; *Schindler and Birn*, 1993; *Sanny et al.*, 1994; *Pulkinnen et al.*, 1994; *Pritchett and Coroniti*, 1994; *Hesse et al.*, 1996; *Birn and Schindler*, 2002], reaching length scales comparable with the intrinsic ion scales. In this scenario a thin current sheet leads to a tearing mode or a microinstability.

This type of scenarios assumes that the near-Earth plasma sheet is stable from

the point of view of ideal MHD, at least in the early stages of the substorm growth phase. Indeed, numerical MHD simulations indicate the absence of any pronounced ideal-MHD instability [e.g. *Birn et al.*, 1996]. However, a general stability analysis covering arbitrary modes does not seem to be available. It is the aim of this paper to deal with this problem.

Generally, such an investigation is a difficult task, which might explain why most studies are limited to particular modes. However, in this paper we exploit the fact that general MHD stability results can be obtained in a simple way by selecting a special class of equilibria. To take advantage of that possibility, we choose equilibrium configurations with translational invariance with respect to the cross-tail direction (y-direction) and set the y-component B_y of the equilibrium magnetic field to zero. Under these conditions it suffices to study the ballooning regime to reach a complete assessment of MHD stability with respect to arbitrary modes.

In principle, this allows us to reinterpret existing ballooning stability results for 2D equilibria with vanishing B_y as being valid from a general MHD point of view. However, the corresponding literature does not provide a clear answer. Both stable [*Lee and Wolf*, 1992; *Lee*, 1999a] and unstable [*Bhattacharjee et al.*, 1998; *Miura*, 2001; *Cheng and Zaharia*, 2004] cases have been found, and it has remained unclear what equilibrium parameters control the stability properties and what are the precise conditions under which instability occurs. In particular, the effect of a constant background pressure has not yet been considered. The results of *Lee and Wolf* [1992] indicate that the interchange criterion based on flux tube entropy provides a necessary stability criterion for ballooning. However, sufficiency remains

unclear.

The present study includes background pressure and assesses sufficiency of the entropy criterion. A set of rather simple quantitative stability criteria is derived.

We emphasize that for choices of the equilibrium more general than the present choice the significance of the ballooning results for arbitrary modes is likely to get lost. Nevertheless, ballooning studies under more general conditions have provided valuable pieces of information. The effect of including B_y was studied by *Hurricane* [1997] who found that B_y can have a destabilizing effect. *Lakhina et al.* [1990] established that shear flow can excite highly oscillatory modes. Recently, *Cheng and Zaharia* [2004] presented numerical results on ballooning modes in a three-dimensional equilibrium modelling a substorm growth phase configuration [*Zaharia and Cheng*, 2003] and concluded that it was unstable, although the unstable regime varied according to various stability approaches. Our results allow us to identify a possible reason for the discrepancies between the different results (section 5). The Interchange mode was studied by *Golovchanskaya and Maltsev* [2003], who found that cross-tail variations of the equilibrium, related to field-aligned currents, could destabilize.

In other studies plasma models beyond ideal MHD were used. *Hurricane et al.* [1995], *Lee* [1999b], and *Horton et al.* [2001] took into account kinetic effects, such as caused by drifts and stochastic motion of particles. *Lee* [1999a] concluded that for strongly stretched configurations the addition of the Hall-term does destabilize an otherwise stable configuration, however, *Zhu et al.* [2003] arrived at the opposite conclusion.

The main justification for using ideal MHD in this study is the (qualitative)

overlap between the collisionless plasma regime and ideal MHD in the regime of large spatial and temporal scales [*Schindler and Birn*, 2002]. Further, ideal MHD stability would indicate the non-ideal nature of an observed instability. Also, as ideal MHD is a widely used plasma model, it is of interest to contribute to the clarification of its stability properties.

We begin with a brief review of the implications of ballooning stability for ideal-MHD stability in general, followed by a discussion of some useful properties of the variational principle for ballooning modes. Then, stability of several different equilibrium models is investigated by numerical minimization of $w(A_1)$. Finally, an analytical approach leads to simple stability criteria and identifies the relevant parameters determining the stability of strongly stretched tail equilibria.

2. Background

We choose cartesian coordinates x, y, z with x pointing tailward, z northward and y dawnward and consider magnetohydrostatic systems with $\partial/\partial y = 0$ and $B_y = 0$ for the equilibrium quantities while the perturbations are kept fully three-dimensional. The equilibrium magnetic field is represented by the flux function $A(x, z)$ such that $\mathbf{B} = \nabla A \times \mathbf{e}_y$. Note that for an appropriate tail field, in the center of the plasma sheet A increases in the tailward direction.

Our stability analysis is based on the integral

$$w(A_1) = \frac{1}{2\mu_0} \int \left(\left(\frac{\partial A_1}{\partial s} \right)^2 + V_c A_1^2 + \frac{1}{J^2 \overline{q}} \left(\overline{V_c A_1} \right)^2 \right) \frac{ds}{B}. \tag{1}$$

The expression (1) is defined for each field line separately. The trial function $A_1(s)$ is the linear perturbation of the magnetic flux function, which by $A_1 = -\xi \cdot \nabla A$

involves the perpendicular component of the displacement vector ξ, and s is the arc length on the selected field line. J is given by $\mu_0 j_y$ where j_y is the y-component of the equilibrium current density, which is related to the equilibrium plasma pressure p by

$$j_y = \frac{dp}{dA} \,, \tag{2}$$

J and p are functions of the equilibrium flux function A alone. (Note that equilibrium quantities do not have subscripts.)

The quantity V_c is defined as

$$V_c = -\frac{2\mu_0}{B^2}\kappa \cdot \nabla p \tag{3}$$

where $\kappa = \mathbf{b} \cdot \nabla \mathbf{b}$ with $\mathbf{b} = \mathbf{B}/B$ is the field line curvature vector, and

$$q = \frac{1}{\mu_0 \gamma p} + \frac{1}{B^2} \tag{4}$$

with γ being the polytropic index. The bar denotes the following average

$$\overline{(\cdots)} = \frac{\int (\cdots) ds/B}{\int ds/B} \,. \tag{5}$$

$A_1(s)$ is subject to line-tying boundary condition, such that $A_1 = 0$ at the points where the selected field line passes through the boundary of the region under consideration (see Fig. 1 with $\tau(s) = s$).

The equilibrium possesses the symmetry $A(-z) = A(z)$, which implies that the eigenmodes are either symmetric or antisymmetric. The symmetry also allows to confine spatial integrations to $z \geq 0$, with the boundary condition $\partial A_1/\partial s$ or $A_1 = 0$ at $x = v, z = 0$ for symmetric or antisymmetric modes, respectively. For antisymmetric modes $\overline{V_c A_1}$ vanishes.

Several authors have used the functional $w(A_1)$ in connection with MHD stability for compressible modes. From the general variational expression for ideal MHD [*Bernstein et al.*, 1958], *Schindler et al.* [1983] derived a variational principle for 2D equilibria including a B_y-component and a gravity force. The expression (1) was obtained by setting B_y and the gravity force to zero, by ignoring a positive term and by minimizing with respect to ξ_y and $\xi_\parallel = \xi \cdot \mathbf{B}/B$ (Appendix of *Schindler et al.* [1983]). From the derivation it follows that a sufficient stability criterion is provided when $w(A_1) > 0$ is satisfied for all trial functions A_1. *De Bruyne and Hood* [1989], starting out from the general expression of *Schindler et al.* [1983], derived two new expressions. In the first case they omitted a positive term and thus obtained a sufficient stability criterion. In the second they applied the ballooning limit [e.g. *Freidberg*, 1987], thereby obtaining a necessary stability criterion. *De Bruyne and Hood* [1989] observed the remarkable property that both expressions coincide for $B_y = 0$ (for a related discussion see also *Hameiri et al.* [1991]).

We have investigated the resulting criterion further and we could establish that in the absence of gravity the corresponding variational integral can be reduced to (1). Thus, under the present equilibrium conditions (2D, $B_y = 0$, no gravity), nonnegative $w(A_1)$ for all admissible trial functions is necessary and sufficient for stability with respect to arbitrary ideal MHD modes. Apparently, the ballooning mode is the most unstable mode so that its absence guarantees stability for arbitrary ideal MHD modes.

We refrain from presenting our derivation here explicitly. Instead, in the Appendix we outline the derivation of a general 3D ballooning functional, which immediately reduces to (1) for the present class of 2D equilibria. For sufficiency

we refer (1) by *Schindler et al.* [1983]. *Lee and Wolf* [1992] gave an independent derivation of $w(A_1)$ for ballooning modes.

The Euler-Lagrange equation for variation of (1) with the normalizing constraint

$$\frac{1}{2\mu_0}\int A_1^2\frac{ds}{B} = C, \tag{6}$$

where C is a positive constant, is given by

$$-B\frac{\partial}{\partial s}\left(\frac{1}{B}\frac{\partial A_1}{\partial s}\right) + V_c A_1 + \frac{V_c}{J^2\overline{q}}\overline{V_c A_1} = \lambda A_1 \ , \tag{7}$$

with λ denoting the eigenvalue. The lowest eigenvalue, λ_{min}, equals $w(A_1)/C$ with the minimizing mode inserted for A_1.

The eigenvalue problem was considered by *Hurricane* [1997], *Bhattacharjee et al.* [1998], *Lee* [1999b] and by others for selected cases.

We add a remark concerning the role of entropy. It is well-known that the spatial variation of entropy

$$S = \ln(pW^\gamma), \quad W = \int \frac{ds}{B} \ , \tag{8}$$

where W is the flux tube volume, provides important information on stability [*Rosenbluth and Longmire*, 1957]. In particular, it applies to interchange modes [*Krall and Trivelpiece*, 1973]. This criterion was applied to the magnetotail by *Hurricane et al.* [1995]. They found interchange instability for the linear equilibrium model (see model 1 of the following section).

There is an important connection between the expression (1) and entropy as was shown by *Lee and Wolf* [1992]. This is based on a relationship that can be written as

$$J^2\overline{q} + \overline{V_c} = \frac{J^2}{\mu_0\gamma}Q \ , \tag{9}$$

where

$$Q = \frac{dS}{dp} + c_b, \quad c_b = \frac{\gamma}{JW}\left[\frac{1}{B^2}\frac{\mathbf{n}_b \cdot \nabla A}{\mathbf{n}_b \cdot \mathbf{B}}\right]_{s_b} \tag{10}$$

where $\mathbf{n}_b$ is the outward-pointing normal of the earthward boundary (Fig. 1) and $s = s_b$ the point where the field line under consideration passes through that boundary. The term c_b is a correction, which in typical magnetospheric configurations is negligibly small, as long as $\mathbf{n}_b \cdot \mathbf{B}$ is sufficiently bounded away from zero. If the boundary is placed at the actual ionosphere, it is the large value of B on the boundary that makes c_b small [*Lee and Wolf*, 1992]. If, instead of the actual ionospheric boundary we use a boundary in the near-Earth tail region, which is meant to represent the ionospheric boundary qualitatively, $c_b = O(\epsilon^2)$ in typical cases. (Here, $\epsilon \ll 1$ measures the aspect ratio of the stretched plasma sheet, see the following section.) For example, the vertical boundary shown in Fig 1 gives

$$c_b = \frac{\gamma}{JW}\left[\frac{B_z}{B^2 B_x}\right]_{z_b} \tag{11}$$

with B_z and $1/W$ of order ϵ. We will ignore c_b when discussing numerical results, however, c_b is kept in the more general discussions by using Q instead of dS/dp.

The equation (9) can be obtained by using the equilibrium condition $\nabla(\mu_0 p + B^2/2) - \mathbf{B} \cdot \nabla \mathbf{B} = 0$ in (3) which gives

$$Vc = -\mathbf{e}_y \cdot \nabla \times \left(\frac{J\mathbf{B}}{B^2}\right) - \frac{J^2}{B^2} - \frac{dJ}{dA}. \tag{12}$$

Applying Stokes's theorem to the area bounded by a field line, the x-axis and the near-Earth boundary (Fig. 1) and differentiating the result by A gives (9).

If $Q < 0$, one finds immediately that

$$w(A_1) > w^*(A_1) \tag{13}$$

with

$$w^* = \frac{1}{2\mu_0} \int \Big(\left(\frac{\partial A_1}{\partial s} \right)^2 + V_c A_1^2 - \frac{\left(\overline{V_c A_1} \right)^2}{\overline{V_c}} \Big) \frac{ds}{B} \tag{14}$$

where $\overline{V_c}$ is assumed to be negative due to the large negative peak at the field line vertex. The functional w^* was introduced as a lower bound on the ballooning criterion for interchange-stable configurations [*Lee and Wolf*, 1992].

It was shown by *Horton et al.* [2001] that (14) is a valid lower bound also for a variety of other plasma models, taking into account kinetic effects, such as caused by drifts and stochastic motion of particles [*Hurricane et al.*, 1995].

3. Numerical minimization of $w(A_1)$

Here we investigate the stability of 3 different equilibrium models from the point of view of ideal MHD by minimizing the function $w(A_1)$ numerically. The first part describes general aspects that apply to all 3 models jointly.

General model aspects

The degree of stretching is described by a characteristic aspect ratio $\epsilon \ll 1$, which measures the ratio of the equilibrium length scales in z- and x-directions. In the numerical procedure the stretching is taken out of the x-coordinate by replacing it by $x_1 = \epsilon x$. In this paper we emphasize strongly stretched configurations.

As the running coordinate along a given field line we replace s by a coordinate $\tau(s)$, $d\tau/ds > 0$ (Fig. 1), defined separately for each model. A, τ are not necessarily orthogonal coordinates. The field line intersects the left boundary at $x = x_0$ and the vertex is located at $x = v, z = 0$, see Fig. 1.

From here on, dimensionless quantities are used, such that $\mathbf{B}$ is normalized

by a typical lobe field strength B_0, pressure by B_0^2/μ_0, lengths by a characteristic scale length L of the plasma sheet in the z-direction, J by B_0/L, A by $B_0 L$, V_c by $1/L^2$ and w by $B_0 L/\mu_0$. The frequency is normalized by the inverse of the Alfvén wave transit time $L\sqrt{\mu_0\rho_0}/B_0$ where a constant density ρ_0 has been assumed. The notation of non-dimensional variables is kept unchanged.

For reasons of reference we give the non-dimensional forms of (1):

$$w(A_1) = \frac{1}{2}\int \left(\left(\frac{\partial A_1}{\partial s}\right)^2 + V_c A_1^2 + \frac{1}{J^2\,\overline{q}} \left(\overline{V_c A_1}\right)^2 \right) \frac{ds}{B} \,, \tag{15}$$

The form of (7) is unchanged.

As the sign of the eigenvalue, which is in the focus of this work, is independent of the normalization condition, the normalizations different from (6) are used for convenience. If not stated otherwise, we use

$$\frac{1}{2}\int A_1^2 \, d\tau = 1. \tag{16}$$

Interpreting the eigenvalue as the square of the frequency ω would require using $\int \rho\xi^2/2 d^3r$ as the normalization integral. Even then the resulting values of ω^2 would be correct only if the perturbation is concentrated on a single field line, which cannot be expected to represent an actual magnetospheric perturbation. Therefore, it seems acceptable to replace the exact normalization integral by a simplified version where ξ is replaced by its perpendicular component, which leads to the choice

$$\frac{1}{2}\int \frac{A_1^2}{B^2}\frac{ds}{B} = 1. \tag{17}$$

When we give values of ω, they are computed with (17). In that case the perturbation of the flux function is denoted by a.

Although, typically the pressure gradient plays an important destabilizing role in stretched field configurations, as it is evident from (3), it is important to note that this does not apply to a constant background pressure p_0, which does not contribute to the gradient. In fact, for symmetric modes, p_0 has a stabilizing influence. This is obvious from the fact, that p_0 enters $w(A)$ only through the quantity $\overline{q}$. The background pressure has no effect on antisymmetric modes, as the compressibility-term is absent.

In the numerical minimization procedure, the trial function $A_1(\tau)$ is represented by a finite Fourier series, satisfying the boundary conditions. The value of γ is set to 5/3. The minimizing mode is determined by minimizing $w(A_1)$ with respect to the Fourier coefficients with the norm condition taken into account. The sign of the minimum of w determines stability.

It must be realized that this kind of straightforward minimization does not identify members of a possible continuum part of the spectrum. This, however, does not seem to cause a major difficulty, as we can assume that according to Grad's hypothesis [e.g. *Freidberg*, 1987] the continuum would be confined to the stable regime.

The number of Fourier modes was varied from 12 to 120 to achieve a relative accuracy that typically was better than 0.001.

model 1

The first model is characterized by the familiar linear solution of the Grad-Shafranov equation [*Voigt*, 1986]. Here we follow *Birn et al.* [2003], who used the following form of the linear solution, including a background pressure, p_0, as a

starting configuration for a numerical simulation.

The magnetic flux function is given by

$$A = -\frac{2}{\pi}\,\cos(\frac{\pi}{2}z)\,e^{-x_1} \quad \text{for } 0 \le z \le 1, \tag{18}$$

$$A = \frac{1}{\epsilon}\sin(\epsilon(z-1))\,e^{-x_1} \quad \text{for } z > 1, \tag{19}$$

with $x_1 = \epsilon x$ and $A(-z) = A(z)$.

The plasma pressure is

$$p = \frac{A^2}{2}\left(\frac{\pi^2}{4} - \epsilon^2\right) + p_0 \quad \text{for } 0 \le z \le 1, \tag{20}$$

$$p = p_0 \quad \text{for } z > 1. \tag{21}$$

The magnetic field components obtained from (18) are

$$B_x = -\sin(\frac{\pi}{2}z)\,e^{-x_1} \tag{22}$$

$$B_z = \frac{2\epsilon}{\pi}\cos(\frac{\pi}{2}z)\,e^{-x_1} = -\epsilon A\,. \tag{23}$$

This model overlaps with the one used by *Hurricane* [1997] for their ballooning analysis. The present model is more general by the inclusion of the background pressure p_0 and an open flux region, but more special by excluding B_y.

An example of a set of magnetic field lines is shown in Fig. 2. The horizontal field line corresponds to $A = 0$ separating closed ($A < 0$) from open ($A > 0$) magnetic flux.

We begin by considering the region of closed flux described by (18) and (20).

Setting $x_0 = 0$, the model parameters are p_0 and ϵ or suitable combinations thereof. We choose ϵ and the pressure ratio $K = p_0/p_m$, where $p_m = (1 - 4\epsilon^2/\pi^2)/2 + p0$ is the maximum pressure in the domain considered.

As the minimization is carried out for each field line separately, the value A marking the selected field line is a further parameter. For the present case of closed field lines it is convenient to replace A by the x_1-coordinate of the vertex, $v_1 = \ln(-2/(\pi A))$. Minimization runs were done for parameter sets in the regime $0.0001 \leq \epsilon \leq 0.3$, $0 < v_1 \leq 4$ and $0 \leq K \leq 1$, using the norm condition (17).

First, let us look at symmetric modes A_1. The most interesting feature was found to be the presence of an unstable region embedded in an extended region of stability. Fig. 3 illustrates that feature in the K, v_1-plane for $\epsilon = 0.01$. The points are the result of minimizations, iterated for vanishing eigenvalues. The smooth curve corresponds to the marginal entropy criterion $dS/dA = 0$. The differences are smaller than the resolution of the graph.

The coincidence of the actual marginal states with those predicted by the entropy criterion was surprising. From the results of *Lee and Wolf* [1992] one could have expect stability for $Q < 0$. But apparently, in the present case $Q < 0$ is not only sufficient but also necessary for stability, at least to an excellent approximation. An explanation is provided in section 4.

As expected, the background pressure, represented by the parameter K, stabilizes. As the figure indicates, there is no instability for K larger than a critical value near 0.002, the value obtained from the entropy criterion is 0.00197.

The points of marginal stability were found to be practically unchanged for smaller values of ϵ. This feature holds exactly for the entropy criterion. The

entropy is given by

$$S = \ln\left\{\left(e^{-2v_1} + \frac{K}{1-K}\right)\left(e^{v_1}\arccos(e^{-(v_1-x_{10})})\right)^{5/3}\right\} + \ln\left\{\frac{1}{2\epsilon^{5/3}}\left(1-\frac{4\epsilon^2}{\pi^2}\right)\right\}, \tag{24}$$

which shows that $dS/dv_1 = 0$ (and therefore $dS/dp = 0$) is independent of ϵ.

Consistent with the entropy criterion, there is no indication from the minimizations for stability transitions in addition to those shown in Fig. 3.

All antisymmetric modes that were investigated in a scan of parameter space were found stable.

Let us look at a case with an unstable symmetric mode in detail, choosing $\epsilon = 0.1, K = 0$, $v_1 = 2$. The symmetric and antisymmetric minimizing modes $a(z)$ are shown in Fig. 4

The symmetric mode is sharply peaked at the vertex, where it responds to the strong curvature. As the antisymmetric mode is forced to vanish at the vertex, it explores the region of large curvature less effectively, which stabilizes.

The region of open flux region ($A > 0$) is trivially stable. There is no pressure gradient, which is evident from (21), such that $V_c = 0$ and $w(A_1)$ becomes positive definite.

Model 2

The flux function of the second equilibrium model that we studied is given by

$$A(x,z) = \ln \frac{\cosh\left[\left(1+\frac{1}{\sqrt{2(r_1+x_1)}}\right)z\right]}{\sqrt{1+\frac{\sqrt{r_1+x_1}}{\sqrt{2}\,r_1}+\frac{1}{4r_1}}} \tag{25}$$

where $r_1 = \sqrt{{x_1}^2 + {z_1}^2}$, $x_1 = \epsilon x$, $z_1 = \epsilon z$. This case belongs to the class of solutions of the Grad-Shafranov equation characterized by current density (y-component)

and pressure

$$J = -e^{-2A}, \quad p = \frac{1}{2}e^{-2A} \; . \tag{26}$$

Although the corresponding Grad-Shafranov equation

$$\Delta A = e^{-2A} \tag{27}$$

is nonlinear, it has a well-known general analytic solution, originally found by Liouville in the context of hydrodynamics [*Liouville*, 1853]. In fact (27) is solved by

$$A = \ln \frac{1 + |f(\zeta)|^2}{2|df(\zeta)/d\zeta|} \tag{28}$$

where $f(\zeta)$ is an arbitrary function of the complex variable $\zeta = x + iz$.

To obtain (25) we have chosen $f(\zeta) = \exp(i(\zeta + \sqrt{\zeta/\epsilon}))$. Again, closed field lines are characterized by ϵ and v_1, where v_1 is the x_1-coordinate of the vertex.

An example for the magnetic field structure is shown in Fig. 5.

Kan [1973] used the same method with a different generating function $f(\zeta)$. That model, however, although reproducing the tail structure in a qualitatively correct way, shows a rather fast pressure decay along the tail, varying from $p(x_1, 0) = 0.5/x_1^4$ for $x_1 \ll 1$ to $p(x_1, 0) = 0.5 + 1/x_1^2$ for $x_1 \gg 1$. As observations indicate a weaker pressure variation [*Behannon*, 1968], we prefer the present model which has the asymptotic pressure laws $p(x_1, 0) = 0.125/x_1$ for $x_1 \ll 1$ and $p(x_1, 0) = 0.5 + 0.5/\sqrt{x_1}$ for $x_1 \gg 1$.

In a first step we discuss the role of the tail asymptotic theory, which, for symmetric sheets, consists of an expansion with respect to ϵ^2. Other than for model 1, with its rather simple expressions, such an expansion would provide a substantial simplification for strongly stretched ($\epsilon \ll 1$) sheets.

Generally, symmetric solutions of (27) can be written as [*Schindler*, 1972]

$$A = \ln\left(\frac{\cosh(F(x_1)z)}{F(x_1)}\right) + O(\epsilon^2). \tag{29}$$

Expanding (25) in a power series with respect to ϵ, one finds that in the present case F has the form

$$F(x_1) = 1 + \frac{1}{2\sqrt{x_1}}\,. \tag{30}$$

Clearly, (29) with (30) is considerably simpler than the exact expression (25).

However, there is an apparent difficulty. The expansion is *regular* in the sense of singular asymptotics, which implies that in lowest order B^2 is set to B_x^2, because $B_z^2 = O(\epsilon^2)$. This gives uniformly valid expressions for the magnetic field components and current density in leading order. But it fails for computing the curvature term, because the regular expression of V_c diverges at $z = 0$. A singular expansion technique would be a possible answer. Here we suggest a simpler method, which avoids splitting the integration interval into two regions with different integrands.

As the problem arises from B^2 only, it seems natural to keep B^2 in its exact form $B^2 = B_x^2 + B_z^2$ in spite of $B_z^2 = O(\epsilon^2)$. To leading order, this gives the correct answer in the regular region, where $B_x^2 \gg B_z^2$, and has the appropriate asymptotic representation in the singular layer. In other words, we insert (29) with (30) into the exact variational integral $w(A_1)$.

For an example, we illustrate this procedure by making an explicit comparison between the exact and approximated models, setting $\epsilon = 0.01$, $x_{10} = 0.2$, $v_1 = 0.6$. For dealing with (25) we use $\tau = z$ as the coordinate along field lines and choose 14 Fourier modes for representing the trial function $a(z)$, which is taken as

antisymmetric. The minimization gives $\omega^2 = 0.001464$. The same problem is treated with the asymptotic method described above. Its simpler structure suggests to set $\tau = u$, where u is defined by

$$u = 2\sqrt{F(x_1) - F(v_1)};. \tag{31}$$

In this case the minimization gives $\omega^2 = 0.001466$. The difference of the two results is mainly due to numerical errors such as the error caused by the finite number of modes.

In view of such good agreement we have used the approximate version to obtain the following results.

A systematic set of minimization runs were carried out for $\epsilon = 0.01$ and $\epsilon = 0.001$ and v_1 varied from 0.6 to 3.0 in steps of 0.6. The earthward boundary point was placed at $x_1 = 0.2$. The resulting frequencies are shown in Fig. 6. All cases shown have positive ω^2 and hence are stable. The frequencies scale with ϵ approximately as $\omega \propto \epsilon$, where this scaling improves with increasing v_1.

The frequencies for symmetric and antisymmetric modes are also approximately equal. Fig. 7 shows that this is consistent with the eigenmode structure. In the left panel, giving the full u-range, the difference between the symmetric and the antisymmetric eigenmodes is hardly recognizable. The main distinguishing feature is that near the origin, in the thin layer with large field line curvature, the modes adjust to their respective boundary condition (right panel of Fig. 7). Outside that layer the deviations are small, even decreasing with increasing v_1, such that the differences of frequencies are no longer visible in Fig. 6 for $v_1 \geq 1.2$.

As v_1 increases, the strong curvature of the symmetric mode near the vertex

(Fig. 7) leads to increasing gradients near the origin, such that an increasing number of Fourier modes was required for achieving the desired accuracy and the computations became more and more time-consuming. (Therefore we did not include the symmetric modes for $v_1 = 2.4$ and $v_1 = 3.0$.)

In contrast to model 1 no unstable parameter region was detected for model 2 for symmetric modes. Again, this turns out to be consistent with the entropy criterion, as can be seen from the monotonic increase of entropy with A (corresponding to $dS/dp < 0$) shown in Fig. 8. In the limit of small ϵ the curves $S(A)$ practically become independent of ϵ. In view of the stability of the investigated equilibria a background pressure was not included.

For studying open field lines x_10 was set to 0.2 and the system was artificially closed at $x_1 = 4$, ϵ was chosen to 1/10 and to 1/100. The flux function value was varied from 0 to 2.79 corresponding to $0.65 \leq z \leq 2.00$ at $x_1 = x_{10}$. All cases were stable. As expected, field line curvature was not important. For an example, at $A = 2.79$ the contributions w_1, w_2, w_3 (first, second and third term, respectively)) to the minimum of w in (15) give the ratios $w_2/w_1 = -1.08 \cdot 10^{-3}$ and $w_3/w_1 = 2.38 \cdot 10^{-8}$, such that the magnetic energy term (w_1) strongly dominates. Again, ω scales as ϵ very well. This is consistent with the longest standing Alfvén wave that fits between the boundaries.

Model 3

In the third model, again, we use the tail-asymptotic version (29) of the Liouville solutions. We observe that the pressure on the x_1-axis, $\hat{p}(x_1)$, is given by

$\hat{p}(x_1) = F(x_1)^2/2$ and use a power law for $\hat{p}(x_1)$,

$$\hat{p}(x_1) = \frac{1}{{x_1}^n}, \quad n > 0 \; . \tag{32}$$

For testing reasons (see section 4) we include values of n above 2, although the corresponding equilibrium solutions are not realistic from the magnetospheric point of view [*Schindler and Birn*, 1982]. The location of the left boundary was set to $x_{10} = 1$. With the choice (32) all field lines are closed.

In view of the encouraging experience gained with applying the entropy criterion, let us see what it predicts in the present case. First, we set the background pressure to zero. Fig. 9 shows $S(v_1)$ for values of n ranging from 1 to 14.

The figure suggests that equilibria with $n < 10$ are stable from the entropy point of view (tailward increase of S), whereas cases with $n > 10$ possess unstable flux tubes. (Note that the limiting condition, i.e. $n = 10$, also applies to the existence of steady state convection in the far tail [*Schindler and Birn*, 1982], as for $n = 10$ and large v_1 the entropy S approaches a constant value).

We tested the relevance of the entropy criterion by a set of minimization runs. Here, the following property must be taken into account. As n approaches 10 from above, the maximum of the curves $S(v_1)$ shift to increasing values of v_1 (Fig. 9). To keep the problem within the regime of large vertex curvature, an increase of v_1 would require a decrease of ϵ. The latter makes the problem increasingly difficult from the numerical point of view. Therefore, we chose moderate value of v_1, taking into account that the stability transition does not occur exactly at $n = 10$, but slightly above. For the parameters chosen the entropy criterion predicts a marginal

state at $n = 10.89$.

The minimization runs with $n = 1, 2...14$ for symmetric modes gave a stability transition (in the anticipated direction) between n=10 and n=11. A local set of runs with n spaced by 0.05, located the transition between 10.85 and 10.90, in excellent agreement with the entropy criterion. For antisymmetric modes, runs with $n = 1, 2...5$ gave stability, and runs with $n = 6, 7...14$ instability. The latter were the only cases of unstable antisymmetric modes that we found. Note, however, that, as mentioned above, they lie in a regime that is unrealistic from the magnetospheric point of view.

For reasons of confirmation we tested whether a sufficiently large background pressure can stabilize the unstable symmetric modes in the way found for model 1. For that purpose we choose $n = 14$. The prediction of the entropy criterion can be obtained from Fig. 10. The figure indicates a stability transition near $K = 0.0001$, where again $K = p_0/p_m$. A set of minimization runs near $v_1 = 1.46$ with varying K again confirmed that transition.

4. Analytical considerations

The stability properties of models 1-3, as far as investigated, seem to have several features in common. For symmetric modes and small ϵ there is consistency with the entropy criterion ($Q < 0$ necessary and sufficient for stability) within the numerical or plotting accuracy; antisymmetric modes were found stable except for the (rather unrealistic) regime $n > 6$ of model 3. Here we attempt to arrive at a better understanding of these properties by analytical considerations. This is done by deriving a set of simplified stability criteria, which do not require numerical

minimization nor solving an eigenvalue problem.

We confine the discussion to the region of closed field lines with higher pressure on their concave side, so that $\kappa \cdot \nabla p > 0$, implying that the curvature potential (3) is negative. For convenience, we choose the running coordinate along field lines as $\tau = \int_0^s B ds$, and write the perturbation A_1 as $\alpha(\tau)$. Also, we are interested only in determining stability or instability rather than in finding growth rates. Then the norm of the perturbation used to determine the Euler-Lagrange equation (7) can be chosen arbitrarily. We choose

$$\frac{1}{2}\int_0^{\tau_b} \alpha^2 \phi d\tau = 1, \tag{33}$$

where τ_b corresponds to the near-Earth boundary and

$$\phi = -\frac{V_c}{B^2}. \tag{34}$$

The length of the field line is $s_b = O(1/\epsilon)$, implying that τ_b is of order $1/\epsilon$ also.

4.1. Symmetric modes

Dealing with symmetric modes we use the abbreviations

$$D := \frac{1}{J^2 \int q ds/B} \tag{35}$$

and

$$Y = \int_0^{\tau_b} \phi \alpha d\tau. \tag{36}$$

Then, (7) assumes the form

$$\ddot{\alpha} + (1+\lambda)\phi\alpha = D\phi Y, \tag{37}$$

where the dot denotes differentiation with respect to τ. The boundary conditions

are $\dot{\alpha}(0) = 0, \alpha(\tau_b) = 0$. Note that due to the different norms the eigenvalues λ of (7) and (37) are different, however the signs of the minimum eigenvalues agree.

We also need to consider the associated homogeneous eigenvalue problem

$$\ddot{\eta} + \sigma\phi\eta = 0, \quad \dot{\eta}(0) = 0, \quad \eta(\tau_b) = 0. \tag{38}$$

Note that, in contrast to (37), the problem (38) is a Sturm-Liouville eigenvalue problem with the corresponding typical properties [e.g. *Morse and Feshbach*, 1953], some of which we briefly summarize. Consider the eigenvalue problem (38) in the full interval $-\tau_b < \tau < \tau_b$ and let the eigenvalues σ_ν, which are real, be arranged in ascending order, such that $\sigma_0 < \sigma_1 < \sigma 2...$ Then symmetric modes correspond to even ν and antisymmetric modes to odd ν. Also, the eigenfunction η_ν has ν internal zeros. None of these properties can be expected to hold for the eigenvalues of the integro-differential equation (37).

The equation (37) may be solved in two steps [*Hurricane*, 1997]. First we set $Y = 1$ and find a solution of (37) for arbitrary values of λ, except for the values $\lambda = \sigma_\nu - 1$, where the solution has singularities. Then (36) returns Y as a function of λ and the eigenvalues follow from the equation

$$Y(\lambda) = 1. \tag{39}$$

Conveniently, the solution of (37) with $Y = 1$ is expressed in terms of the solution $u(\tau, \lambda)$ of the homogeneous equation

$$\ddot{u} + (1 + \lambda)\phi u = 0 \tag{40}$$

understood as an initial value problem with initial conditions $u(0, \lambda) = 1, \dot{u}(0, \lambda) =$

0. Then, the solution of (37) with $Y = 1$ is

$$\alpha(\tau, \lambda) = \frac{D}{1+\lambda}\left(1 - \frac{u(\tau, \lambda)}{u_b(\lambda)}\right) \tag{41}$$

with $u_b(\lambda) = u(\tau_b, \lambda)$. With he help of (40), integrated from 0 to τ_b, this gives

$$Y(\lambda) = \frac{DZ}{1+\lambda} + \frac{D}{(1+\lambda)^2}\frac{\dot{u}_b(\lambda)}{u_b(\lambda)} \tag{42}$$

where $Z = \int_0^{\tau_b} \phi d\tau$ and $\dot{u}_b(\lambda) = \dot{u}(\tau_b, \lambda)$.

As shown below, for small ϵ (42) assumes a rather simple structure. If ϵ is sufficiently small, the second term of (42) is significant only in small intervals of λ containing a singularity at $\lambda = \sigma_\nu - 1$, (corresponding to vanishing u_b). Outside those regions $Y(\lambda)$ can therefore be approximated by the first term,

$$Y_0(\lambda) = \frac{DZ}{1+\lambda} \tag{43}$$

which gives an eigenvalue

$$\lambda_Q = DZ - 1. \tag{44}$$

With (9) λ_Q can be written as

$$\lambda_Q = -\frac{Q}{\gamma \bar{q}}. \tag{45}$$

Here, we have ignored the exceptional case where λ_Q falls inside one of singular structures. It will become clear later that the likelihood of these cases strongly decreases with decreasing ϵ. Similarly, exceptional eigenfunctions of (37) with vanishing integral (36) are excluded by setting Y to 1. Both exceptions are merely the consequence of simplifications, they are physically insignificant and they can be avoided by small changes of parameters.

As $Y_0(\lambda)$ is a monotonic function, all eigenvalues other than (44) must be associated with the singularities of (42) arising from zeros of u_b.

An example of the function $Y(\lambda)$ is given in Fig. 11, showing Y for model 3 with $n = 2, x_{10} = 1$, $v_1 = 2$ for two values of ϵ. The figure also indicates that, outside the singularities, the expression (43) (smooth curves) is a good approximation, particularly for the smaller value of ϵ. The graph includes the singularity at $\lambda = \sigma_2 - 1$. In the case $\epsilon = 0.3$ the resolution used in the figure is sufficient to show the singularity at $\lambda = 1.208$. For $\epsilon = 0.1$ the singular structure (around the singularity at $\lambda_2 = 0.584$) is so thin that it is hardly visible.

The narrow structure of the singular parts of $Y(\lambda)$ and other details can be understood in terms of the following properties, which are derived in the Appendix:

$$\begin{aligned} 0 < \sigma_0 &= O(\epsilon^3), \quad 0 < \sigma_2 = O(1), \quad \lambda_{min} \geq \sigma_0 - 1 \\ \lambda_Q &= O(\epsilon), \quad \delta\lambda_n = O(\epsilon^3),\ n = 0, 2, \ldots \end{aligned} \tag{46}$$

where λ_{min} is the minimum eigenvalue of (37) and $\delta\lambda$ characterizes the width of the thin structures of $Y(\lambda)$ associated with the singularities.

These properties immediately lead to the following conclusions regarding the minimum eigenvalue λ_{min}. For $\nu = 2, 4, \ldots$, each eigenvalue σ_ν generates an eigenvalue $\lambda_\nu = \sigma_\nu - 1 + O(\epsilon^3)$, because as u_b passes through zero, the singular part of $Y(\lambda)$ assumes all values between $-\infty$ and $+\infty$, such that there is a point with $Y(\lambda) = 1$ inside a small neighborhood of $\lambda = \sigma_\nu - 1$. The case $\nu = 0$ is different, because of the presence of the singularity of the first term in (42) at $\lambda = -1$. From (46) one concludes that there is no eigenvalue λ to the left of the singularity ($\lambda < \sigma_0 - 1$). The singular structure to the right of the singularity again has a width of order ϵ^3. Thus, the curve $Y(\lambda)$ returns to the smooth background shape in a range where $\lambda + 1 = O(\epsilon^3)$. There $Y = O(1/\epsilon^3)$, implying that in the vicinity

of the singular structure associated with σ_0 the values of Y stay far above 1, so that there is no λ-eigenvalue in that region. This means that for λ_{min} we find

$$\lambda_{min} = \min(\lambda_Q, \lambda_2). \tag{47}$$

If we ignore the small difference of order ϵ^3 between λ_2 and $\sigma_2 - 1$, this criterion reduces to

$$\lambda_{min} = \min(\lambda_Q, \sigma_2 - 1). \tag{48}$$

Thus, the stability problem is reduced to determining whether σ_2 is smaller or larger than $\lambda_Q + 1$. In view of the Sturm-Liouville properties of (38) this can be done by simply plotting $u(\tau, \lambda_Q)$. If that curve has not more than one internal (i.e. in $0 < \tau < \tau_b$) zero point, then $\lambda_{min} = \lambda_Q$, if it has two or more internal zeros then $\lambda_{min} = \sigma_2 - 1$. Thus, for small ϵ the stability analysis with respect to symmetric modes is reduced to computing λ_Q and plotting a single solution of an initial value problem. No minimization nor iterations are necessary. In view of (46), for sufficiently small ϵ it suffices to investigate $u(\tau, 0)$ instead of $u(\tau,\ \lambda_Q)$.

Fig. 12 shows a corresponding analysis for model 1. In all cases shown $u(\tau, 0)$ has one zero only, such that for symmetric modes $\lambda_{min} = \lambda_Q$ holds. This explains the excellent coincidence between numerical results and the entropy criterion in Fig. 3.

We note that $\lambda_{min} = \lambda_Q$ does not only apply to model 1. All symmetric mode results described in section 3 are consistent with $\lambda_{min} = \lambda_Q$, such that $Q < 0$ is necessary and sufficient for stability. Possibly, this property has an even more general significance.

It might seem puzzling that stability turns out to be determined by Q,

which depends on p and W, quantities that do not particularly involve the strong curvature at the vertex. (They remain bounded for $\epsilon \to 0$.) The explanation is that the dominant contributions from curvature and compressibility cancel each other. This follows from (44) which can be written as

$$\lambda_Q = -\frac{1}{J^2\bar{q}}(\bar{V}_c + J^2\bar{q}). \tag{49}$$

Both $\bar{V}_c$ and $J^2\bar{q}$ are of order $1/\epsilon$, the leading terms being $-\overline{J^2/B^2}$ and $\overline{J^2/B^2}$ (see (12) and (4)), which cancel each other, such that $\lambda_Q = O(\epsilon)$.

4.2. Antisymmetric modes

For antisymmetric modes the boundary conditions are $\alpha(0) = 0$, $\alpha(\tau_b) = 0$. Considering the full range $-\tau_b \le \tau \le \tau_b$ the integral (36) vanishes such that on the interval $0 \le \tau \le \tau_b$ one deals with the eigenvalue problem (37) with $Y = 0$. Thus, $\alpha_n(\tau) = \zeta_n(\tau)$ and $\lambda_n = \sigma_n - 1$, n=1,3,..., where ζ_n satisfies

$$\ddot{\zeta} + \sigma\phi\zeta = 0, \quad \zeta(0) = 0, \quad \zeta(\tau_b) = 0. \tag{50}$$

The eigenvalues of (38) and those of (50) are ordered as

$$\sigma_0 < \sigma_1 < \sigma_2 < \sigma_3 < \dots \tag{51}$$

Thus, for antisymmetric modes the minimum eigenvalue is

$$\lambda_{min} = \sigma_1 - 1. \tag{52}$$

Analogous to the symmetric case, the sign of $\sigma_1 - 1$ can be determined from a single solution of an initial value problem. Here that initial value problem is

$$\ddot{v} + (\lambda + 1)\phi v = 0, \quad v(0) = 0, \quad \dot{v}(0) = 1, \tag{53}$$

solved by $v(\tau, \lambda)$. If $v(\tau, 0)$ has no internal (i.e. $0 < \tau < \tau_b$) zero point, then $\lambda_{min} > 0$, if $v(\tau, 0)$ has one or more internal zeros then $\lambda_{min} < 0$.

There is an interesting sufficient stability criterion for antisymmetric modes, stated as follows: Let B_z be symmetric and B_x antisymmetric with respect to z and consider a field line A. If

$$\{B_x B_z \neq 0,\ B_x B_z \frac{\partial^2 B_z^2}{\partial A \partial z} \leq 0\} \quad \text{for} \quad z > 0 \tag{54}$$

on that field line, then the field line is stable with respect to antisymmetric modes. A proof of this criterion is given in the Appendix. It directly proves stability of antisymmetric modes of model 1, where B_z is constant on field lines.

5. Summary and Discussion

We studied the ideal-MHD stability of two-dimensional magnetotail configurations with large field line curvature at the field line vertices subject to arbitrary three-dimensional perturbations. We regard this case as relevant for the Earth's magnetotail in the limit of small particle gyro-radii. MHD-stability would explain the presence of periods during which the plasma sheet thickness is large compared with a typical ion gyro-radius (evaluated in the lobe magnetic field) and the disturbance level is small and the bulk flow velocities remain well below the Alfvén velocity (computed with typical values of density in the plasma sheet center and of the lobe magnetic field strength).

We emphasize that the understanding of the preonset quiescent states is an important key to magnetospheric activity, and, in particular, substorms. If the tail is found ideal-MHD stable, an observed instability must involve non-MHD effects,

which would be an important piece of evidence.

Even in cases where a significant fluctuation level is present observationally, it is still appropriate to choose a quiet state as the equilibrium in a stability analysis. If one finds instability one might be able to explain the fluctuations on that basis.

The equilibria that we studied are magnetohydrostatic with translational invariance with respect to the cross-tail direction (y-direction) and $B_y = 0$. The perturbations have no geometric restriction except that the displacement vector ξ vanishes on the boundary, qualitatively representing a highly-conducting solid ionosphere. This is a good approximation when the timescale for the evolution of the instability is short compared to resistive diffusion times at the ionosphere.

First we have addressed the (known) fact that, under these conditions, the general MHD-stability problem can be reduced to the problem of stability with respect to the ballooning mode alone. Then we discussed the connection between the ballooning criterion and the entropy criterion known from the study of interchange modes. That criterion predicts stability (instability) for tailward increase (decrease) of entropy $S = \ln(pW^\gamma)$.

By numerical minimization we studied the stability of three equilibrium models, a linear model (in which the current density depends linearly on the flux variable), a nonlinear model constructed by the Liouville-method and a model based on the tail-asymptotic expansion with a power law for the pressure variation along the tail axis. In each case numerical minimizations were performed for a variety of parameters and the entropy criterion was evaluated. The parameters were chosen such that in all cases the closed field lines had strong curvature at the vertex. This generally requires strongly stretched configurations.

Our parameter choice for the cases presented in section 3 excludes the near-Earth region, because in this paper we concentrate on the role of the strong curvature at the vertices of closed field lines. Particular attention was paid to the effect of a background pressure.

The results can be summarized as follows.

1. Symmetric modes on closed field lines.

   The stability properties of the symmetric modes on closed field lines was found to be in good agreement with the predictions of the entropy criterion (see e.g. Fig. 3). Model 1 showed an unstable region associated with a weak decrease of the entropy function with distance, but a small background pressure (in our example near or below 1/500 of the maximum pressure) was found to stabilize the instability, consistent with change of the entropy function to monotonic increase with distance. For model 2 all symmetric modes were found stable, and for model 3 symmetric modes are stable for $n < 10$. The instability for $n > 10$ appears to be stabilized by a small background pressure, as established for $n = 14$, where the stabilizing relative pressure p_0/p_m was near 10^{-4}. All of these results were found to be consistent with the entropy criterion.

   Instabilities seem to be associated with rather rapid tailward pressure decay (exponential in model 1 and faster than $1/{x_1}^{10}$ in model 3), which leads to a decreasing entropy function. The more realistic cases with $n < 2$ [e.g. *Behannon*, 1968] were stable in all cases even without the presence of a background pressure. For the more rapidly decaying models the instabilities

are removed by a small background pressure.

2. Antisymmetric modes on closed field lines.

   The antisymmetric modes were found stable, except for model 3 when $n > 6$. Again, instability was found only in the cases of relatively strong tailward pressure decay. For model 1, stability was also shown in general by applying an exact analytical criterion (end of section 4).

3. Open field lines

   Open field lines, which are present in models 1 and 2, were found to be stable in all cases.

4. Growth rates

   For models 1 and 2 we included the evaluation of frequencies or growth rates, using a modified normalization condition (section 3). For model 1 see the example of Fig. 4. For model 2, where no instability was found, we investigated the dependence of the lowest frequency on the vertex location v_1, on ϵ, and on mode symmetry. We found that, approximately for small ϵ, ω/ϵ depends only on v_1. This is consistent with the longest standing Alfvén wave fitting between the boundaries.

These results give support to the view that there are considerable domains in parameter space of stretched magnetotail configurations that are ideal-MHD stable. Instabilities seem to be confined to configurations with rather fast tailward pressure decay, were pressure is understood as a function of $x_1 = \epsilon x$. Perhaps, MHD-stability is a determining factor for the rather moderate tailward pressure

decrease, as observed.

The stabilizing effect of a background pressure arises, because the background contributes to the stabilizing compressibility effect without affecting the destabilizing curvature term. This aspect seems to be relevant for assessing the role of the ballooning instability for magnetospheric substorms. In view of the smallness of the background pressure required for stabilization, the residual plasma pressure in the tail lobes might well have a significant effect. Perhaps even more importantly, our results suggest that the pressure of a wide plasma sheet, in which a thin current sheet is embedded, has an effect similar to a constant background pressure, and hence would have a stabilizing effect for the thin current sheet. Further studies are required for a quantitative assessment of these effects.

For the conditions of central interest of the present paper, i.e. the regime of strongly stretched closed field lines with $\kappa \cdot \nabla p > 0$, the stability properties have been expressed in terms of a few simple criteria. Stability is determined by the entropy function $S(p)$ and the signs of σ_1, σ_2, where σ_n, $n = 0, 1, 2, \ldots$, are the eigenvalues of a simplified problem (homogeneous Euler-Lagrange equation). $S(p)$ is available from integrations of known functions along field lines and the signs of σ_1 and σ_2, in each case, can be found from a single solution of an initial value problem (i.e. (40) or (53), respectively), which is much more easy to solve than the original eigenvalue equation or the minimization problem. Combining the results for symmetric and antisymmetric modes one finds that for sufficiently small ϵ it is necessary and sufficient for MHD-stability that

$$\min(\lambda_Q, \sigma_1 - 1) > 0 \tag{55}$$

where the sign of λ_Q is determined by the sign of $-dS/dp$.

The numerical results are fully consistent with (55). For symmetric modes the less stringent criterion (48) holds. Possibly, there is a criterion that is even simpler than (48), because, remarkably, in all numerical examples we found

$$\sigma_2 - 1 > \lambda_Q. \tag{56}$$

If that inequality held generally, the interchange criterion $dS/dp < 0$ would be necessary and sufficient for ideal-MHD stability of symmetric modes under the present assumptions.

Our results can give a number of plausible explanations of the differences between the various results on the ballooning instability in the literature. *Lee and Wolf* [1992] looked at symmetric modes using Kan's model [*Kan*, 1973] and a local model where $B_x \propto z$ and B_z constant. They found stability in both cases. It is easy to confirm that Kan's model has $dS(p)/dp < 0$, so that, provided that (56) holds in that case also, it is stable with respect to symmetric modes. The local configuration corresponds to a linear decay of B^2 with x_1, which is a rather weak decay compared with the decays that led to instability, so that our results would suggest stability. *Hurricane et al.* [1995] found interchange instability of the linear model (without background pressure) in agreement with our model 1.

In their treatment of the ballooning mode using Kan's model, *Miura et al.* [1989] found instability of the symmetric mode. *Lee and Wolf* [1992] suggested that the reason was their setting $\mathbf{B}\cdot\xi = 0$, for which *Lee and Wolf* [1992] did not see a justification. Our results give support to the latter view. In a more recent paper, *Miura* [2000] showed that setting $\mathbf{B}\cdot\xi$ to zero is equivalent to neglecting the

compressibility term (third term in the integrand of (1)). This would correspond to setting $D = 0$ in (37). Clearly, that choice would render all our examples unstable, because then $\lambda = \sigma_0 - 1$ would become the lowest eigenvalue, which, because of (46) would be negative in all cases for sufficiently small ϵ. Having found several cases, where the symmetric mode is stable, we conclude that compressibility is important and cannot be neglected. Possibly, the reason for this discrepancy is that, as mentioned by *Miura* [2000], their scaling breaks down near the vertex. The sharp peak of the unstable mode at the vertex, (e.g. Fig. 4) might emphasize the vicinity of the vertex enough for the scaling violation to have significant consequences.

Bhattacharjee et al. [1998] studied the stability of ballooning modes for configurations that developed during a driven evolution. For the symmetric compressible mode they found instability in some cases. The eigenmode was sharply peaked as in Fig. 4. As in some cases we found instability too, and in the absence of detailed information about the field structure of the quasi-equilibria, their results are not necessarily inconsistent with ours. Our findings would raise the question, though, whether that instability might disappear if a suitable background pressure was superimposed.

Birn et al. [2003] used the same equilibrium as that of the present model 1 in a numerical study of the propagation of bubbles. The authors did not see any evidence for a ballooning instability. Our results indeed confirm stability in their case. Model 1 is stabilized by background pressure for a value of K above 0.002 (Fig. 3). The background pressure $p_0 = 0.025$ used by *Birn et al.* [2003] corresponds $K = 0.048$ (for $\epsilon \ll 1$ and $x_{10} = 0$) and thus their equilibrium lies in the stable regime.

In a recent study, *Cheng and Zaharia* [2004] found instability for a 3-D equilibrium modelling a substorm growth phase configuration [*Zaharia and Cheng*, 2003] over a wide spatial range. However, applying the Lee and Wolf [1992] criterion, which is consistent with our criterion, they found instability within a more limited region. This region is characterized by a local decrease of the entropy function with radial distance from the Earth [Zaharia, private communication], consistent with our findings. In contrast, the more extended unstable region in the general approach apparently results from their choice of ionospheric boundary condition $\nabla \cdot \xi = 0$. As shown in the Appendix, with the present normalization that boundary condition implies that the compressibility term vanishes along the entire field line. This applies to both the two-dimensional (1) and the three-dimensional (A17) functional. The vanishing of the compressibility term has a strong destabilizing effect. (See the remark on *Miura et al.* [1989]).

Occasionally one encounters the intuitive argument that due to the large field line curvature, close magnetotail field lines should be ballooning unstable. This is not supported by our findings. On the contrary, the stability properties of the high-β plasma sheet is the result of a subtle balance between thermal and magnetic energy, which cannot be predicted by simply pointing at the curvature. Also, a small constant background pressure can have a strong stabilizing effect.

We emphasize that our investigation was centrally aimed at strongly stretched configurations. Less stretched equilibria may well behave differently. In particular, the ballooning instability was inferred to occur in the transition region from the tail to the dipole region [*Roux et al.*, 1991; *Cheng and Zaharia*, 2004].

Our findings confirm that under typical conditions a close relationship exists

between ballooning unstable regimes and a (perhaps localized) decrease of the entropy function S with distance from the Earth. This result puts constraints on the evolution toward ballooning instability during the substorm growth phase. If the evolution starts from a configuration with monotonically increasing S and is governed by adiabatic (i.e., isentropic) ideal MHD the entropy function S remains unchanged, even if a local embedded current sheet is formed [*Birn and Schindler*, 2002]. The development of a ballooning unstable region hence requires violation of ideal MHD and/or entropy conservation.

Appendix: Derivations

Here we give the derivations of a number of properties used in section 4.

Symmetric modes

In this part we derive the properties (46).

All eigenvalues σ_n are positive as follows by multiplying (38) with η_n and integrating with respect to τ, which gives

$$\sigma_n = \frac{\int_0^{\tau_b} \dot{\eta}^2 d\tau}{\int_0^{\tau_b} \phi\eta^2 d\tau}. \tag{A1}$$

Next, we estimate the magnitude of σ_0 and σ_2. Typically, ϕ is strongly localized to a region of scale $\tau_1 = O(\epsilon^2)$ while $\tau_b = O(1/\epsilon)$. Thus, beyond a few time τ_1 each eigenmode η_n approaches a straight line (see Fig. A1). The denominator in (A1) can be estimated by an appropriate rescaling, introducing new zero-order quantities. Let $\phi = \tilde{\phi}/\epsilon^4$ (because $V_c = O(1/\epsilon^2)$, $B^2 = O(\epsilon^2)$) and $\tau = \tilde{\tau}\epsilon^2$ such that $\tilde{\tau}_1 = \tau_1/\epsilon^2$ becomes of order 1. Then with $\eta = \tilde{\eta}$ we find $\int_0^{\tau_1} \phi\eta^2 d\tau = 1/\epsilon^2 \int_0^{\tilde{\tau}_1} \tilde{\phi}\tilde{\eta}^2 d\tilde{\tau} = O(1/\epsilon^2)$. The numerator of (A1) scales differently for

$n = 0$ and $n = 2$. In the curvature layer where ϕ is localized, η_0 does not deviate much from 1 and the main contribution to the numerator of (A1) comes from the external region with $|\dot{\eta}| \approx 1/\tau_b$. With these estimates we conclude from (A1) that $\sigma_0 = O(\epsilon^3)$. Unlike η_0 there is strong variation of η_2 inside the curvature layer (Fig A1). The same rescaling as applied to the denominator gives $\int_0^{\tau_b} = O(1/\epsilon^2)$, such that $\sigma_2 = O(1)$.

The fact that $\lambda_{min} > \sigma_0 - 1$ follows from a comparison of the variational integrals associated with (37) and (38).

The magnitude of λ_Q as given by (45) is estimated by observing that Q is a zero order quantity and that $\bar{q} = O(1/\epsilon)$. The latter comes from $\int ds/B = O(1/\epsilon)$ (the main contribution coming from the region outside the curvature layer) and $\int ds/B^3 = O(1/\epsilon^2)$ (the main contribution coming from the curvature layer).

The singular structures of the function $Y(\lambda)$ as given by (42) can be analyzed as follows. Writing Y as

$$Y = \frac{DZ}{1+\lambda}\left(1 + \frac{1}{Z(1+\lambda)}\frac{\dot{u}_b}{u_b}\right) \tag{A2}$$

we set $\lambda = \sigma_n - 1 + \delta\lambda_n$ and impose the condition

$$\frac{1}{Z(1+\lambda)}\left|\frac{\dot{u}_b}{u_b}\right| = 1 \tag{A3}$$

which means that $|Y|$ has returned from ∞ to the order of magnitude of the smooth background. The first task is to express u_b by $\delta\lambda_n$. This can be done by formulating (40) at $\lambda = \sigma_n - 1 + \delta\lambda_n$ and at $\lambda = \sigma_n - 1$. Multiplying each equation by the other solution, integrating with respect to τ and taking the difference of the resulting expressions gives to the leading order in $\delta\lambda_n$

$$\frac{u_b}{\dot{u}_b} \;=\; \delta\lambda_n \frac{\int_0^{\tau_b} \phi\eta_n^2 d\tau}{\dot{\eta}_{nb}^2}$$

$$
\begin{aligned}
&= \delta\lambda_n \frac{\int_0^{\tau_b} \dot{\eta_n}^2 d\tau}{\sigma_n \dot{\eta}_{nb}^{\ 2}} \\
&> \delta\lambda_n \frac{\tau_b}{\sigma_n} \qquad \text{(A4)}
\end{aligned}
$$

where, in the last step we have included only the external contribution to the numerator integral. From (A3) and (A4) one obtains

$$|\delta\lambda_n| < \frac{1}{Z\tau_b(1+\delta\lambda_n/\sigma_n)}. \qquad \text{(A5)}$$

For $\delta\lambda_n > 0$ this gives

$$\delta\lambda_n < \frac{1}{Z\tau_b} = O(\epsilon^3). \qquad \text{(A6)}$$

For $\delta\lambda_n < 0$ we can exclude $n = 0$ because, as seen above, there is no eigenvalue to the left of the singularity at $\sigma_0 - 1$. Therefore we can use $\sigma_n = O(1)$. Then, (A5) has a solution with $\delta\lambda \ll \sigma_n$. Ignoring the term $\delta\lambda_n/\sigma_n$ in the right-hand side we immediately find from (A5) that again $\delta\lambda_n = O(\epsilon^3)$.

Antisymmetric modes

Here we derive the criterion that states stability with respect to antisymmetric modes for equilibria with the property (54).

For antisymmetric modes the variational expression (15) can be written as

$$w(a) = \int_0^{z_b} \left(\frac{B_z}{B^2} \left(\frac{\partial a}{\partial z} \right)^2 + \frac{V_c}{B_z} a^2 \right) dz \qquad \text{(A7)}$$

where all entering functions are understood as functions of z and A. In these coordinates V_c takes the form

$$V_c = -\frac{2J}{B} \frac{\partial}{\partial z} \left(\frac{B_x}{B} \right). \qquad \text{(A8)}$$

We set

$$a(z, A) = B_x B_z \zeta(z, A), \quad \zeta'(0, A) = 0, \quad \zeta(z_b, A) = 0, \qquad \text{(A9)}$$

where the prime symbol means partial differentiation with respect to z.

The present symmetry properties of B_x, B_z imply that the symmetric trial functions ζ correspond to the antisymmetric trial functions a. It is essential that (A9) does not impose any restriction on a, apart from the boundary conditions. This is satisfied by the property $BxBz \neq 0$ for $z > 0$.

Inserting (A9) into (A7) and integrating by parts gives

$$w(\zeta) = \int_0^{z_b} \left(\frac{B_z^3 B_x^2}{B^2} \zeta'^2 - \frac{1}{2} B_x B_z \frac{\partial^2 B_z^2}{\partial A \partial z} \zeta^2 \right) dz, \tag{A10}$$

where we have made use of $J = \mathbf{e}_y \cdot \nabla \times \mathbf{B}$ and $\nabla \cdot B = 0$, using the expressions for the curl and divergence operators as they apply to the present curvilinear coordinates.

By (54) the functional (A10) is positive definite, which completes the proof.

Ballooning modes of three-dimensional equilibria

Here, we derive a general 3D variational functional for the ballooning instability which readily specializes to (1) for the present 2D equilibria.

For that purpose we start from a particular form of the MHD variational principle in *Freidberg* [1987], however, with an important generalization. Freidberg sets the $\nabla \cdot \xi$ term to zero, which he justifies in view of laboratory applications and simplicity. As we show in this paper, in the magnetosphere, the compressibility plays an important role, such that $\nabla \cdot \xi$ is kept in the equation. Setting $\xi = \theta \exp(i\Sigma)$ one finds, using that $\mathbf{B} \cdot \nabla \Sigma = 0$,

$$\nabla \cdot \xi = e^{i\Sigma} (\nabla \cdot \theta_\parallel + \nabla \cdot \theta_\perp + i \theta_\perp \cdot \nabla \Sigma). \tag{A11}$$

Then Equation 10.5 of Freidberg becomes

$$\begin{aligned}\delta W = \frac{1}{2\mu_0}\int d\mathbf{r}\Big[&|\nabla\times(\theta_\perp\times\mathbf{B})_\perp|^2\\ &+\quad B^2|i\mathbf{k}_\perp\cdot\theta_\perp+\nabla\cdot\theta_\perp+2\kappa\cdot\theta_\perp|^2\\ &-\quad 2\mu_0(\theta_\perp\cdot\nabla p)(\theta_\perp^*\cdot\kappa)\\ &-\quad \mu_0 j_\parallel(\theta_\perp^*\times\mathbf{b})\cdot\nabla\times(\theta_\perp\times\mathbf{B})_\perp\\ &+\quad \mu_0\gamma p|\nabla\cdot\theta_\parallel+\nabla\cdot\theta_\perp+i\mathbf{k}_\perp\cdot\theta_\perp|^2\Big],\end{aligned}\tag{A12}$$

where $\mathbf{k}_\perp = \nabla\Sigma$. Introducing the ballooning expansion (large $k_\perp$) with $\theta = \theta_\mathbf{0} + \theta_\mathbf{1} + \ldots$ one finds from minimizing the leading term of the functional that $\theta_{\perp\mathbf{0}}$ has the form $\theta_{\perp\mathbf{0}} = X\mathbf{b}\times\mathbf{k}_\perp/B$ [*Freidberg*, 1987].

In the minimization with respect to $\theta_{\perp 1}$, the compressibility leads to a difference with respect to Freidberg's approach. One finds

$$\begin{aligned}\delta W &= \frac{1}{2\mu_0}\int d\mathbf{r}\Big[k_\perp^2|\mathbf{b}\cdot\nabla X|^2 - 2\mu_0\theta_{\perp\mathbf{0}}\cdot\nabla p\;\theta_{\perp\mathbf{0}}^*\cdot\kappa\\ &+ \frac{1}{q}|\nabla\cdot\theta_\parallel - 2\kappa\cdot\theta_{\perp\mathbf{0}}|^2\Big].\end{aligned}\tag{A13}$$

Minimization of (A13) with respect to $\theta_\parallel$ gives

$$\mathbf{b}\cdot\nabla\left(\frac{\nabla\cdot\theta_\parallel - 2\kappa\cdot\theta_{\perp\mathbf{0}}}{q}\right) = 0\tag{A14}$$

such that

$$(\nabla\cdot\theta_\parallel - 2\kappa\cdot\theta_{\perp\mathbf{0}})/q = f\tag{A15}$$

where f is constant on field lines. By integration along field lines one finds

$$f = -\frac{\overline{2\kappa\cdot\theta_{\perp\mathbf{0}}}}{\overline{q}}.\tag{A16}$$

As X is differentiated with respect to s only, the minimization can be carried out for each field line separately. Inserting (A15) with (A16) into (A13) and expressing

$\theta_{\perp \mathbf{0}}$ by X, one finally obtains

$$\begin{aligned} w_{3D} &= \frac{1}{2\mu_0}\int \Big[k_\perp^2 |\mathbf{b}\cdot\nabla X|^2 \\ &- \frac{2\mu_0}{B^2}(\mathbf{b}\times\mathbf{k}_\perp)\cdot\nabla p\,(\mathbf{b}\times\mathbf{k}_\perp)\cdot\kappa\,|X|^2 \\ &+ \frac{1}{q}\left|\overline{2(\mathbf{b}\times\mathbf{k}_\perp)\cdot\kappa\, X/B}\right|^2\Big]\frac{ds}{B}. \end{aligned} \tag{A17}$$

Assuming the $\mathbf{B}$ can be represented by Euler potentials as $\mathbf{B} = \nabla\alpha\times\nabla\beta$, one can arrange the potentials such that Σ depends on β alone. Then $\mathbf{k}_\perp = \Sigma_\beta\nabla\beta$.

Setting $X_1 = d\Sigma/d\beta X$, (A17) becomes

$$\begin{aligned} w_{3D} &= \frac{1}{2\mu_0}\int \Big[(\nabla\beta)^2 |\mathbf{b}\cdot\nabla X_1|^2 \\ &- \frac{2\mu_0}{B^2}(\mathbf{b}\times\nabla\beta)\cdot\nabla p\,(\mathbf{b}\times\nabla\beta)\cdot\kappa\,|X_1|^2 \\ &+ \frac{1}{q}\left|\overline{2(\mathbf{b}\times\nabla\beta)\cdot\kappa\, X_1/B}\right|^2\Big]\frac{ds}{B}. \end{aligned} \tag{A18}$$

The expression (A17) (or (A18)) is the desired result. Specializing (A17) for two-dimensional equilibria with $B_y = 0$, $\Sigma = \Sigma(y)$, $X = exp(-i\Sigma)A_1/(d\Sigma/dy)$ immediately gives (1).

As in (1) the compressibility gives rise to a stabilizing term involving field line averages. These terms are the direct consequence of the boundary condition $\xi_\parallel = 0$. Had we chosen the boundary condition $\nabla\cdot\xi = 0$ instead, as occasionally used by other authors, the compressibility term would have disappeared. In that case the minimization leads to $\nabla\cdot\xi = 0$ on the entire field line. Note that the latter property is a consequence of the fact that we use normalizations involving only a particular component of ξ, represented by X. The sign of the minimum of the functional (A17) and thus the property of stability or instability is independent of the normalization.

Also, (9) has a 3D generalization, given by

$$\overline{V_{c,3D}} + \bar{q}\left(\frac{\partial p}{\partial \alpha}\right)^2 = \frac{1}{\gamma}\frac{\partial p}{\partial \alpha}\frac{\partial S}{\partial \alpha} \tag{A19}$$

where $V_{c,3D} = -2\mu_0 \partial p/\partial\alpha\, \kappa \times \nabla\beta \cdot \mathbf{B}/B^2$ and p and S understood as functions of α and β.

Acknowledgments. Work at Los Alamos was supported by the U.S. Department of Energy's Office of Basic Energy Sciences through its Geosciences Research Program, by NASA's Sun Earth Connection Theory Program, and by the National Science Foundation through grant ATM-0202306. The authors wish to thank Drs. Michael Hesse and Sorin Zaharia for valuable comments.

References

Angelopoulos, V., et al., Tailward progression of magnetotail acceleration centers: Relationship to substorm current wedge, *J. Geophys. Res.*, *101*, 24,599–24,620, 1996.

Baker, D., T. Pulkinnen, V. Angelopoulos, and W. Baumjohann, Neutral line model of substorms: Past results and present view, *J. Geophys. Res.*, *101*, 12,975–13,010, 1996.

Baker, D., T. Pulkinnen, M. Hesse, and R. L. McPherron, A quantitative assessment of energy storage and release in the magnetotail, *J. Geophys. Res.*, *102*, 7159–7168, 1997.

Behannon, K., Mapping of the earth's bow chock and magnetotail, *J. Geophys. Res.*, *73*, 907, 1968.

Bernstein, I., E. Freeman, M. Kruskal, and R. Kulsrud, An energy principle for hydromagnetic stability problems, *Proc. Roy. Soc., Ser. A*, *244*, 17, 1958.

Bhattacharjee, A., Z. Ma, and X. Wang, Ballooning instability of a thin current sheet in the high-lundquist-number magnetotail, *Geophys. Res. Lett.*, *25*, 861–864, 1998.

Birn, J., Computer studies of the dynamic evolution of the geomagnetic tail, *J. Geophys. Res.*, *85*, 1214, 1980.

Birn, J., and K. Schindler, Thin current sheets in the magnetotail and the loss of equilibrium, *J. Geophys. Res.*, *107*, 1117, 2002.

Birn, J., M. Hesse, and K. Schindler, MHD simulations of magnetotail dynamics, *J. Geophys. Res.*, *101*, 12,939, 1996.

Birn, J., J. Raeder, Y.Wang, R. Wolf, and M. Hesse, On the propagation of bubbles in the geomagnetic tail, *J. Geophys. Res.*, submitted, 2003.

Cheng, C., and S. Zaharia, MHD ballooning instability in the plasma sheet, *Geophys. Res. Lett.*, submitted, 2004.

De Bruyne, P., and A. Hood, Bounds on the ideal MHD stability of line-tied 2-d coronal magnetic fields, *Solar Physics*, *123*, 241–269, 1989.

Freidberg, J., *Ideal Magnetohydrodynamics*, Plenum Press, New York and London, 1987.

Golovchanskaya, I., and Y. Maltsev, Interchange instability in the presence of the field-aligned current: Application to the auroral arc fromation, *J. Geophys. Res.*, *108*, doi:10.1029/2002JA009505, 2003.

Hameiri, E., P. Laurence, and M. Mond, The ballooning instability in space plasmas, *J. Geophys. Res.*, *96*, 1513, 1991.

Hesse, M., and K. Schindler, The onset of magnetic reconnection in the magnetotail, *Earth Planets Space, Terra Scientific, Tokyo*, *53*, 645–53, 2001.

Hesse, M., D. Winske, M. Kuznetsova, J. Birn, and K. Schindler, Hybrid modeling of the formation of thin current sheets in magnetotail configurations, *J. Geomagn. Geoelec.*, *48*, 749, 1996.

Horton, W., H. Wong, J. van Dam, and C. Crabtree, Stability properties of high pressure geotail flux tubes, *J. Geophys. Res.*, *106*, 18,803–188,022, 2001.

Hurricane, O., MHD ballooning stability of a sheared plasma sheet, *J. Geophys. Res.*, *102*, 19,903–19,911, 1997.

Hurricane, O., R. Pellat, and F. Coroniti, A new approach to low-frequency "MHD-like" waves in magnetospheric plasmas, *J. Geophys. Res.*, *100*, 19,421, 1995.

Kan, J., On the structure of the magnetotail current sheet, *J. Geophys. Res.*, *78*, 3773–81, 1973.

Kaufmann, R. L., Substorm currents: Growth phase and onset, *J. Geophys. Res.*, *92*, 7471, 1987.

Krall, N., and A. Trivelpiece, *Principles of plasma physics*, McGraw-Hill, New York, 1973.

Kuznetsova, M., and L. M. Zelenyi, Collisionless reconnection in collisionless field reversals: The universality of the ion tearing mode, *Geophys. Res. Lett.*, *18*, 1825–1828, 1991.

Lakhina, G. S., E. Hameiri, and M. Mond, Ballooning instability of the earths plasma sheet region in the presence of parallel flow, *J. Geophys. Res.*, *95*, 10,441–10,448, 1990.

Lee, D., Stability analysis of the plasma sheet using Hall magnetohydrodynamics, *J. Geophys. Res.*, *104*, 19,993–9, 1999a.

Lee, D., Effect of plasma compression on plasma sheet stability, *Geophys. Res. Lett.*, *26*, 2705–8, 1999b.

Lee, D., and R. Wolf, Is the earth's magnetotail balloon unstable?, *J. Geophys. Res.*, *97*, 19,251–57, 1992.

Liouville, J., Sur lequation aux differences partielles $\partial^2 log\lambda/\partial u\partial v \pm \lambda/2/a^2 = 0$, *J. de Math. Pures Appl.*, *18*, 71–72, 1853.

Lui, A. T. Y., A. Mankofsky, C. L. Chang, K. Papadopoulos, and C. S. Wu, A current disruption mechanism in the neutral sheet: A possible trigger for substorm expansions, *Geophys. Res.Lett*, *17*, 745–748, 1990.

Mitchell, D. G., D. J. Williams, C. Y. Huang, L. A. Frank, and C. T. Russell, Current carriers in the near-earth cross-tail current sheet during substorm growth phase, *Geophys. Res. Lett.*, *17*, 583, 1990.

Miura, A., Conditions for the validity of the incompressible assumption for the ballooning instability in the long-thin magnetospheric equilibrium, *J. Geophys. Res.*, *105*, 18,793–18,806, 2000.

Miura, A., Ballooning instability as a mechanism of the near-earth onset of substorms, *Space Sci. Rev.*, *95*, 1387–398, 2001.

Miura, A., S. Ohtani, and T. Tamao, Ballooning instability and structure of diamagnetic hydromagnetic waves in a model magnetosphere, *J. Geophys. Res.*, *94*, 15,231, 1989.

Miyashita, Y., S. Machida, T. Mukai, Y. Saito, K. Tsuruda, H. Hayakawa, and P. R. Sutcliffe, A statistical study of variations in the near and middistant magnetotail associated with substorm onsets: Geotail observations, *J. Geophys. Res.*, *105*, 15,913–15,930, 2000.

Miyashita, Y., S. Machida, T. Mukai, Y. Saito, and P. R. Sutcliffe, Mass and energy transport in the near and middistant magnetotail around substorm onsets: Geotail observations, *J. Geophys. Res.*, *106*, 6259–6274, 2001.

Morse, P., and H. Feshbach, *Methods of Theoretical Physics*, McGraw-Hill, New York, 1953.

Pritchett, P. L., and F. V. Coroniti, Convection and the formation of thin current sheets in the near-earth olasma sheet, *Geophys. Res. Lett.*, *21*, 1587, 1994.

Pulkinnen, T., D. N. Baker, D. G. Mitchell, R. L. McPherron, C. Y. Huang, and L. A. Frank, Thin current sheets in the magnetotail during substorms: Cdaw6 revisited, *J. Geophys. Res.*, *99*, 5793, 1994.

Rosenbluth, M., and C. Longmire, Stability of plasma confined by magnetic fields, *Ann. Phys.*, *1*, 120, 1957.

Roux, A., et al., Plasma sheet instability related to the westward traveling surge, *J. Geophys. Res.*, *96*, 17,697, 1991.

Sanny, J., R. L. McPherron, C. T. Russell, D. N. Baker, T. I. Pulkkinen, and A. Nishida, Growth-phase thinning of the near-earth current sheet during the cdaw 6 substorm, *J. Geophys. Res.*, *99*, 5805, 1994.

Schindler, K., A selfconsistent theory of the tail of the magnetosphere, in *Earth's magnetospheric processes*, edited by B. M. McCormac, p. 200, D. Reidel, Dordrecht, The Netherlands, 1972.

Schindler, K., A theory of the substorm mechanism, *J. Geophys. Res.*, *79*, 2803, 1974.

Schindler, K., and Birn, On the cause of thin current sheets in the near-earth magnetotail and their possible significance for magnetospheric substorms, *J. Geophys. Res.*, *98*, 15,477, 1993.

Schindler, K., and J. Birn, Magnetospheric physics, *Phys. Reports*, *47*, 109, 1978.

Schindler, K., and J. Birn, Selfconsistent theory of time-dependent convection in the earth's magnetotail, *J. Geophys. Res.*, *87*, 2263, 1982.

Schindler, K., and J. Birn, Models of two-dimensional embedded thin current sheets from vlasov theory, *J. Geophys. Res.*, in press, 2002.

Schindler, K., J. Birn, and L. Janicke, Stability of two-dimensional pre-flare structures, *Solar Phys.*, *87*, 103, 1983.

Sergeev, V., D. Mitvhell, C. Russell, and D. Williams, Structure of the tail plasma/current sheet at 11 re and its changes in the course of a substorm, *J. Geophys. Res.*, *98*, 17,345, 1993.

Sergeev, V. A., P. Tanskanen, K. Mursula, A. Korth, and R. C. Elphic, Current sheet thickness in the near-earth plasma sheet during substorm growth phase as inferred

from simultaneous magnetotail and ground-based observations, *Adv. Space Res.*, *8*, 125, 1990.

Voigt, G.-H., Magnetospheric equilibrium and slow adiabatic convection, in *Solar Wind and Magnetosphere Coupling*, edited by Y. Kamide and J. Slavin, p. 233, Terra Scientific, Tokyo, 1986.

Zaharia, S., and C. Cheng, Near-earth thin current sheets and Birkeland currents during substorm growth phase, *Geophys. Res. Lett.*, *30*, doi:10.1029/2003GL017456, 2003.

Zhu, P., A. Bhattacharjee, and Z. Ma, Hall magnetohydrodynamic ballooning instability in the magnetotail, *Phys. Plasmas*, *10*, 249–258, 2003.

K. Schindler, Fakultät für Physik und Astronomie, Ruhr-Universität Bochum, 44780 Bochum, Germany. (e-mail: ks@tp4.ruhr-uni-bochum.de)

J. Birn, Space and Atmospheric Science Group, MS D466, Los Alamos National Laboratory, Los Alamos, NM 87545. (e-mail: jbirn.@lanl.gov)

Received _____

This manuscript was prepared with AGU's LaTeX macros v5, with the extension package 'AGU^{++}' by P. W. Daly, version 1.6b from 1999/08/19.

Figure Captions

Figure 1. A field line is characterized by its value A of the flux function and has a running coordinate τ, understood as a function of arclength s. At $x = x_0$, where the field line intersects the left boundary, the perturbation A_1 vanishes. A closed field line (as shown) has a vertex located at $x = v(A), z = 0$.

Figure 2. Field lines of model 1 for $\epsilon = 0.1$.

Figure 3. Stability diagram of model 1 computed for $\epsilon = 0.01$. The square symbols mark the boundary of the unstable region obtained by numerical minimization, the full curve corresponds to the marginal entropy criterion $dS/dA = 0$.

Figure 4. Minimizing modes $a(z)$ for model 1 with $\epsilon = 0.1, K = 0, v_1 = 2$. The symmetric mode is unstable with a growth rate of 0.0173, the antisymmetric mode is stable with a frequency of 0.0158.

Figure 5. Magnetic field lines of model 2 with $\epsilon = 0.1$. The thick field line separates open from closed field lines.

Figure 6. Minimization results for model 2.

Figure 7. Comparison of symmetric and antisymmetric modes for model 2 with $\epsilon = 0.01$, $v_1 = 0.6$.

Figure 8. Entropy S as a function of the flux function value A for model 2, evaluated with (25). Plotted are the curves for $\epsilon = 0.01$, 0.03, 0.1, however, they are indistinguishable.

Figure 9. Entropy S for model 3 as a function of the vertex position v_1 for n ranging from 1 to 14. The curve $n = 10$ separates cases with $dS/dv_1 > 0$ from cases with an interval where $dS/dv_1 < 0$.

Figure 10. Entropy S for model 3 with $n = 14$ as a function of the vertex position v_1 for several values of background pressure parameter K, stabilization occurs near $K = 10^{-4}$. The exact location of the turning point with horizontal tangent is $v_1 = 1.46$, $K = 0.000095$.

Figure 11. The function $Y(\lambda)$ for model 3 with $n = 2$, $x_{10} = 1$, $v_1 = 2$ and $\epsilon = 0.3$ (curve a) and $\epsilon = 0.1$ (curve b). The smooth curves correspond to (43). The dashed vertical lines indicate the positions of the singularity at $\lambda = \sigma_2 - 1$.

Figure 12. Solutions $u(\tau, 0)$ for model 1, computed for 6 parameter pairs (ϵ, v_1). To place all 6 curves into a single diagram we plot $U(\tau) = \tanh(u(\tau, 0))$ instead of $u(\tau, 0)$. All solutions have only one zero.

Figure A1. Qualitative structure of symmetric eigenfunctions η_0 and η_2.

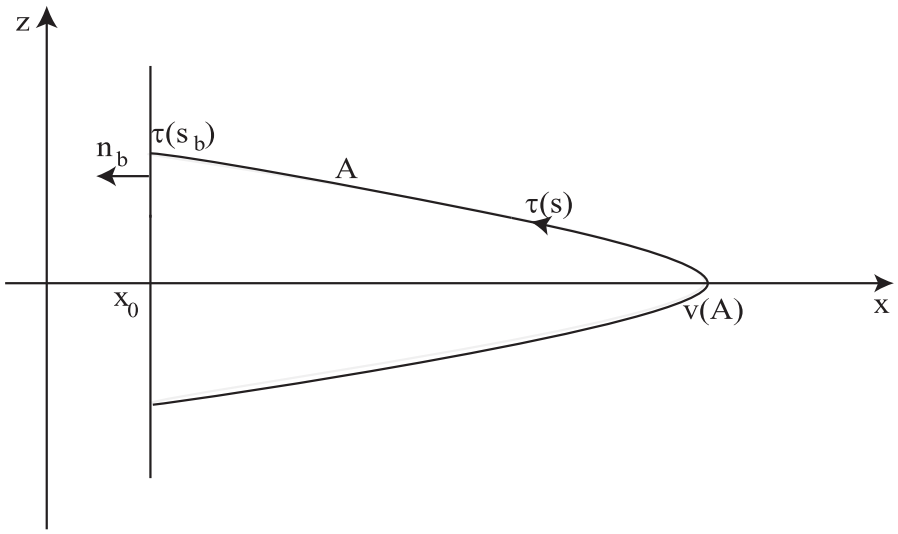

Fig. 1

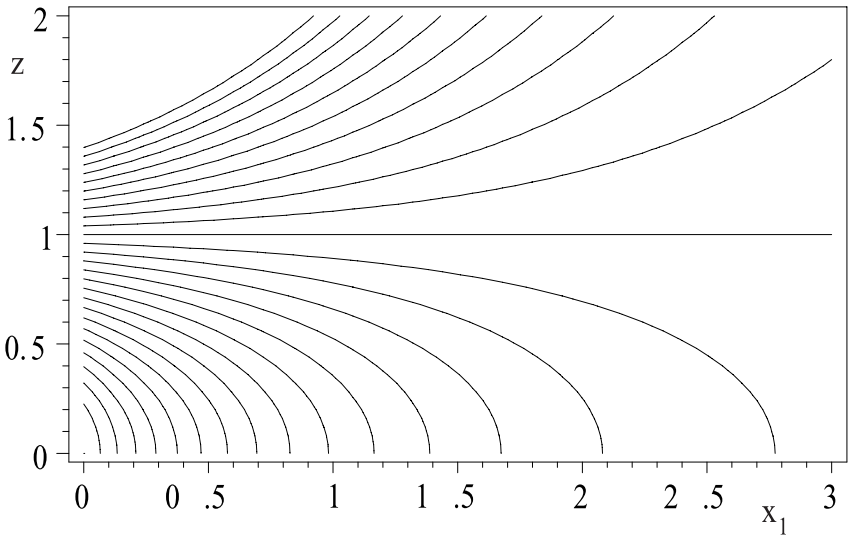

Fig. 2

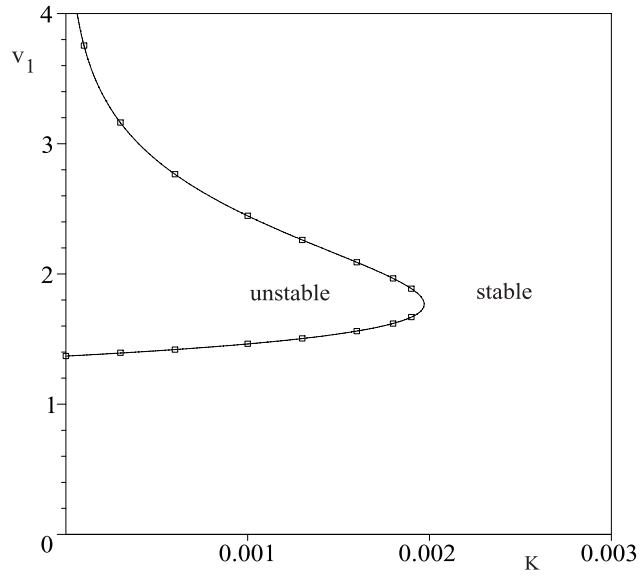
4
v1
3
2
unstable
stable
1
0
0.001
0.002
K
0.003

Fig. 3

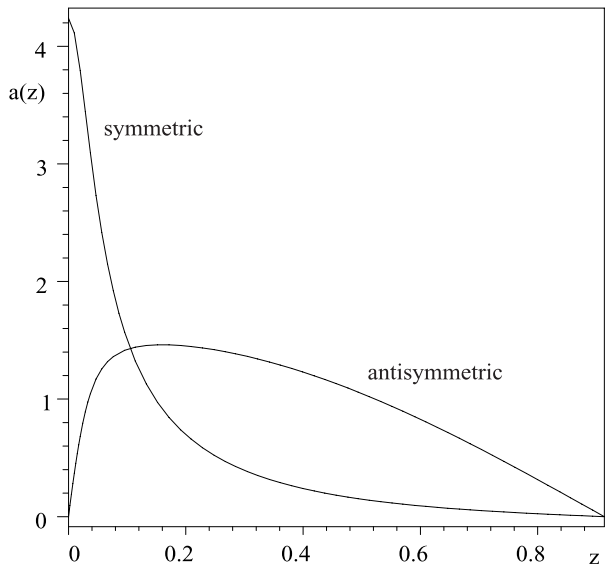
4
a(z)
symmetric
3
2
antisymmetric
1
0
0
0.2
0.4
0.6
0.8
z

Fig. 4

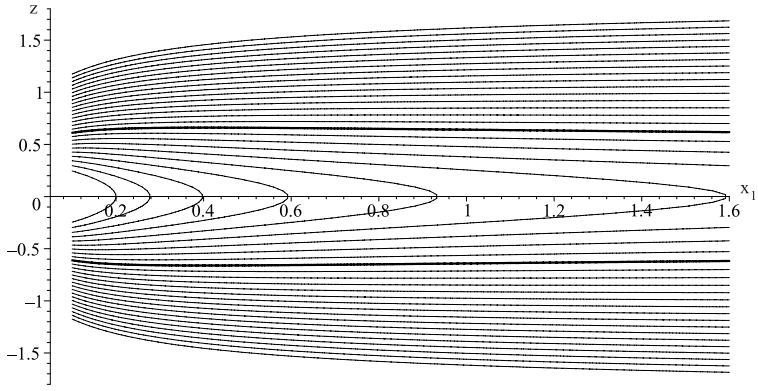
z
1.5
1
0.5
0
–0.5
–1
–1.5
0.2
0.4
0.6
0.8
1
1.2
1.4
1.6
x1

Fig. 5

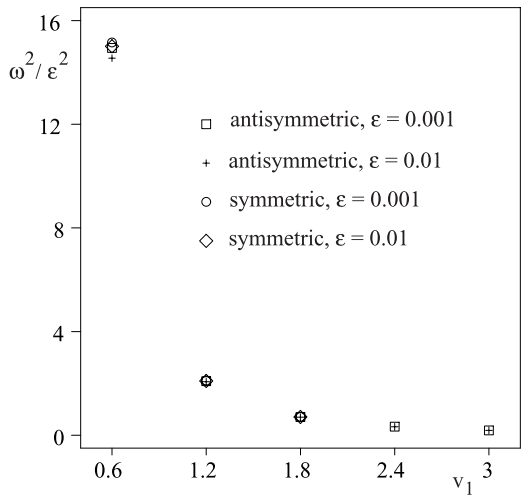
16
12
8
4
0
ω2 / ε2
antisymmetric, ε = 0.001
antisymmetric, ε = 0.01
symmetric, ε = 0.001
symmetric, ε = 0.01
0.6
1.2
1.8
2.4
3
v1

Fig. 6

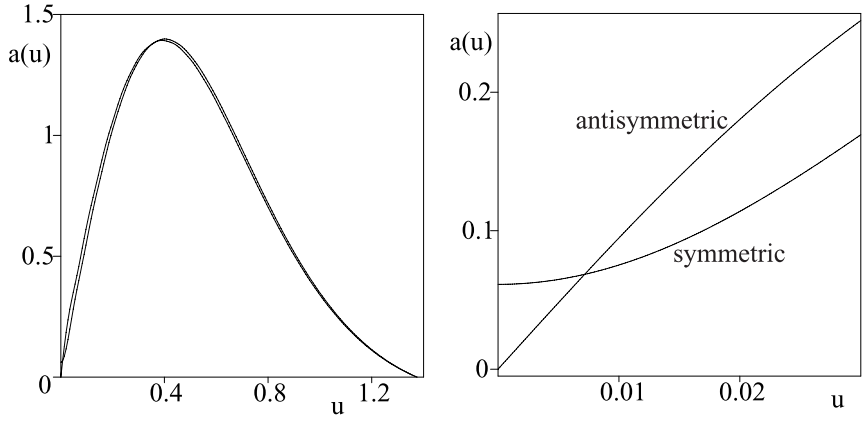
1.5
a(u)
1
0.5
0
0.4
0.8
u
1.2
a(u)
0.2
antisymmetric
0.1
symmetric
0
0.01
0.02
u

Fig. 7

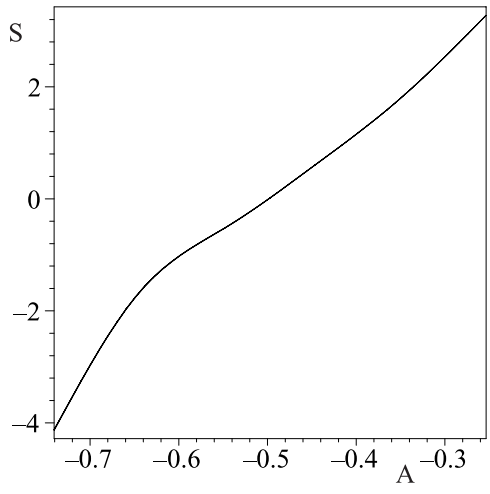
S
2
0
–2
–4
–0.7
–0.6
–0.5
–0.4
–0.3
A

Fig. 8

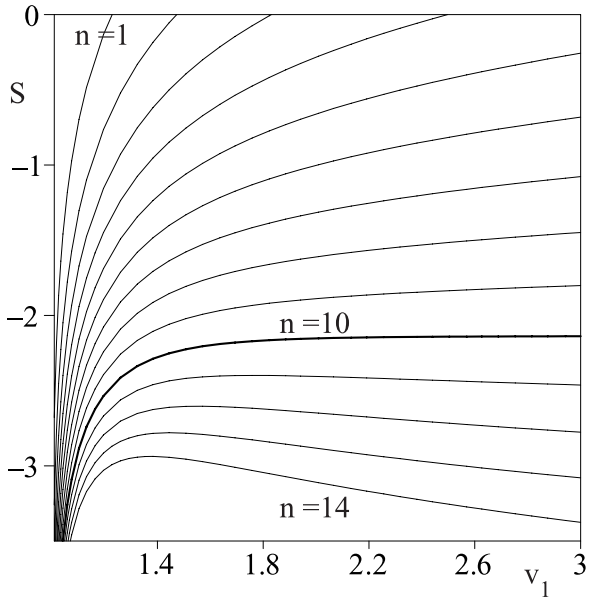
0
n =1
S
–1
–2
n =10
–3
n =14
1.4
1.8
2.2
2.6
3
v1

Fig. 9

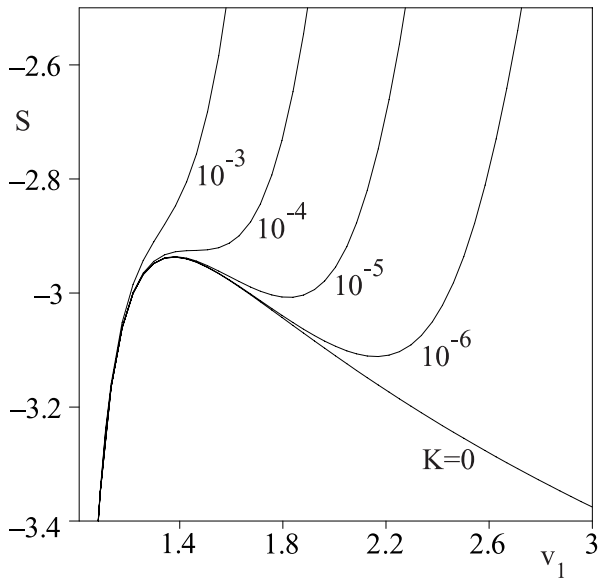
–2.6
S
–2.8
10-3
10-4
10-5
–3
10-6
–3.2
K=0
–3.4
1.4
1.8
2.2
2.6
3
v1

Fig. 10

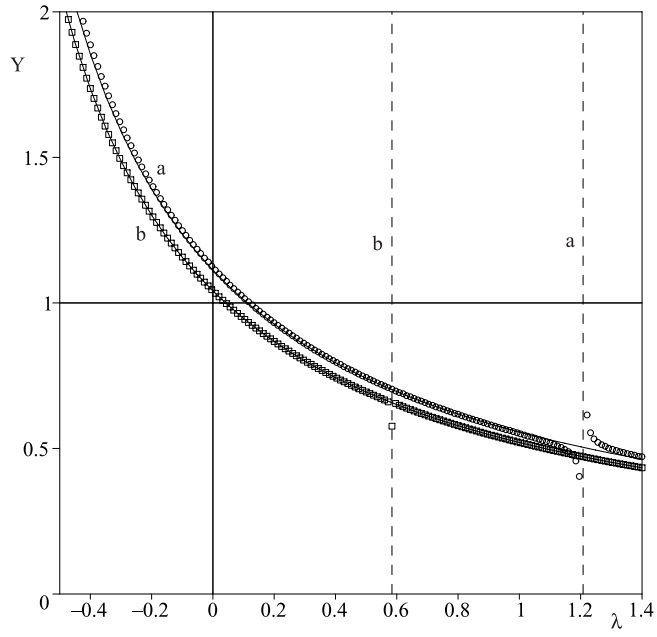
Y
2
1.5
1
0.5
0
a
b
b
a
–0.4
–0.2
0
0.2
0.4
0.6
0.8
1
1.2
1.4
λ

Fig. 11

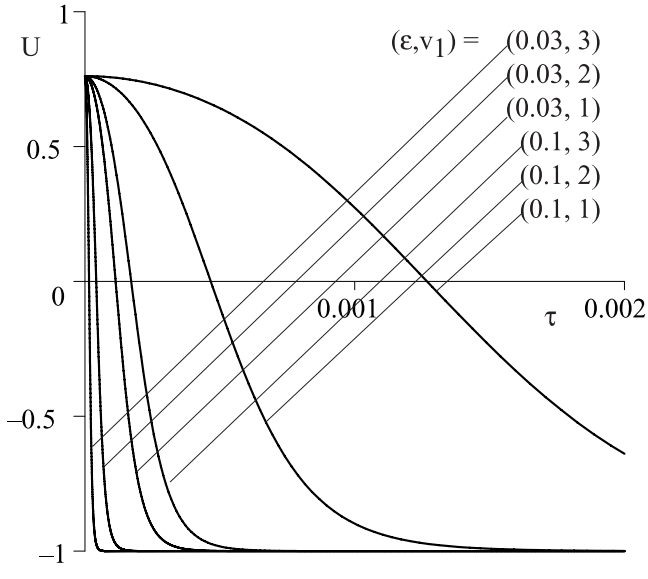
U
1
0.5
0
–0.5
–1
(ε,v1) =
(0.03, 3)
(0.03, 2)
(0.03, 1)
(0.1, 3)
(0.1, 2)
(0.1, 1)
0.001
τ
0.002

Fig. 12

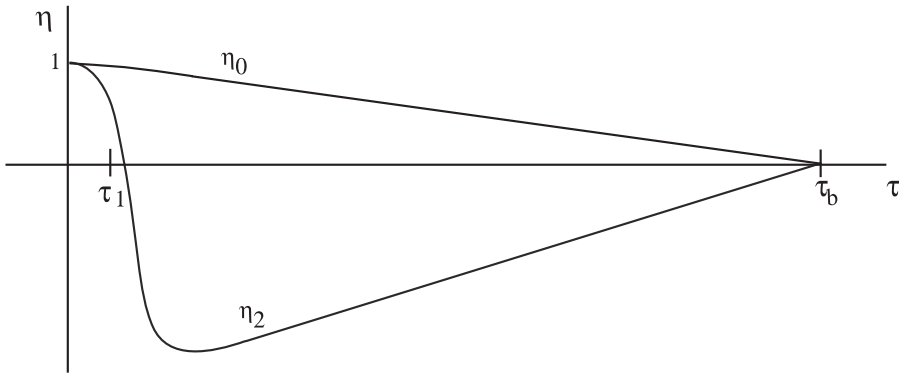

Fig. A1